Multirate Fractional-Order Repetitive Control of Shunt Active Power Filter Suitable for Microgrid Applications

Xie, Chuan; Zhao, Xin; Savaghebi, Mehdi; Meng, Lexuan; Guerrero, Josep M.; Quintero, Juan Carlos Vasquez

Published in:
I E E E Journal of Emerging and Selected Topics in Power Electronics

DOI (link to publication from Publisher):
10.1109/JESTPE.2016.2639552

Publication date:
2017

Document Version
Early version, also known as pre-print

Multi-Rate Fractional-Order Repetitive Control of Shunt Active Power Filter

Chuan Xie, *Member, IEEE,* Xin Zhao, *Student Member, IEEE,* Mehdi Savaghebi, *Senior Member, IEEE,* Lexuan Meng, *Member, IEEE,* Josep M. Guerrero, *Fellow, IEEE,* Juan C. Vasquez, *Senior Member, IEEE*

***Abstract*—This paper presents a multi-rate fractional-order repetitive control (MRFORC) scheme for three-phase shunt active power filter (APF). The proposed APF control scheme includes an inner proportional-integral (PI) control loop with a sampling rate identical to switching frequency and an external plug-in RC loop with a reduced sampling rate. The MRFORC loop is implemented in *dq*-frame with interleaving for the reduction of computational burden in each control cycle. Moreover, in order to deal with the harmonics in the presence of wide grid frequency variations, FORC, which replaces the fractional-order elements with the Lagrange-interpolation based finite impulse response (FIR) filter, is adopted instead of the conventional RC. The synthesis, stability analysis and parameters tuning criteria of the MRFORC system are derived in detail. A step by step design example of the proposed controller is also given in the paper. Finally, experiments are performed to validate the feasibility and effectiveness of the proposed scheme.**

***Index Terms*—Microgrid, active power filter, multi-rate repetitive control, fractional repetitive control.**

I. Introduction

THE existence of nonlinear loads and power electronic equipment has caused severe harmonic pollution in electrical systems. Harmonic currents increase losses, deteriorate the quality of the voltage waveform, cause metering devices malfunction, and may cause resonances and interferences. Active power filters (APFs) that operate as controllable power sources, which have the capability of offering fast response to dynamic load changes are widely used to eliminate power harmonics[1], [2]. Shunt APF is proved to be the most widely used equipment to compensate load current harmonics due to its simplicity, effectiveness and harmonic compensation capabilities[2].

Since the performance of shunt APFs is highly dependent on current control strategy, numerous current control schemes have been proposed in the literature [3]–[12], such as hysteresis control [3], proportional-integral (PI) control [4], [5], proportional resonant (PR) control [6], and deadbeat (DB) control [10], [11]. However, hysteresis control suffers from random switching frequency, DB control is sensitive to parameters change, PI and PR controllers suffer from poor performance in dealing with multiple harmonic currents. Multiple resonant control can achieve zero steady-state tracking error of sinusoidal signals at selected harmonic frequencies[7], [8], [13]. However, a large number of paralleled resonant controllers might cause heavy parallel computation burden and high tuning complexity. Based on the internal model principle[14], repetitive control (RC) [12], [15]–[25] can achieve zero steady-state tracking error for any periodic signal with a known period due to the induced high gains at interested harmonic frequencies. It provides a simple but effective solution for shunt APFs to compensate harmonics.

Conventional digital RC has a simple structures formulated by N delay elements, where N is the number of samples in one fundamental period of the repetitive signal. It is well known that digital RC requires N to be an integer for implementation, but this is not always true in the presence of grid frequency variations, especially under certain circumstances, such as off-grid and remote area condition, the grid frequency may have considerable variation [26]. Variable sampling rate approach enables RC to keep N to be an integer for proper harmonics rejection [22], [27]. However, variable-sampling-rate implies changes of the system dynamics and, particularly the plant model, which more or less increase the difficulty when analyzing the system stability[21]. An alternative way to address this problem is to approximate the fractional part of N by using an interpolation based finite impulse response (FIR) filter [20] or a Lagrange-interpolation-based FIR filter [23], [25], [28]. The fractional delay filter applied in the RC scheme only requires a few multiplications and additions for coefficient updating, and thus, it is suitable for fast online tuning of the fractional-order controller.

Digital control systems which involve more than one sampling frequency are called multi-rate control systems. Compared with single rate control systems, multi-rate control systems have the advantage of appropriate sampling frequency selection, computation saving, and memory reduction. Thus, it can offer a cost-effective solution for converter control systems. Besides, with reduction of sampling rate and computational time, there can be more room for reducing the interruption period and increasing switching frequency, so as to improve the dynamic performance of the converter [29]. Multi-rate RC with

Manuscript received Aug. 22, 2016; revised Oct. 30, 2016; accepted Dec. 7, 2016. This work was supported in part by the Sichuan Science and Technology Support Program 2016GZ0027 and in part by Fundamental Research Funds for the Central Universities ZYGX2014J069 and ZYGX2015J075.

Chuan Xie is with the School of Automation Engineering, University of Electronic Science and Technology of China, Chengdu, 611731, China (e-mail: c.xie@uestc.edu.cn).

Xin Zhao, Mehdi Savaghebi, Lexuan Meng, Josep M. Guerrero and Juan C. Vasquez are with the Department of Energy Technology, Aalborg University, 9220, Denmark (e-mail:{xzh, mes, lme, joz, juq}@et.aau.dk).

down/up-sampling scheme has been applied in areas of motion control [30]. A down-sampled multi-rate scheme for constant voltage constant frequency(CVCF) PWM converters has been investigated in [29]. However, multi-rate frequency-adaptive FORC for APFs has not yet been investigated.

In view of this, in this paper a multi-rate fractional-order repetitive control (MRFORC) scheme is proposed for enhancing APF performance. The MRFORC is proposed to simultaneously address the frequency adaptive issue and to reduce the computation burden. The synthesis, stability analysis and parameters tuning criteria of MRFORC system are developed in Section II. In Section III, experiment test bed is briefly introduced firstly and then a step by step design example of the proposed controller for the given power stage parameters is given. Then the experimental results are provided in Section IV to verify the effectiveness of the proposed MRFORC. Finally, Section V presents the conclusions of the paper.

II. Synthesis of MRFORC

Since the mathematic model of MRFORC is derived from conventional RC, thus the single-rate RC and FORC will be reviewed firstly. Then the equivalent single-rate closed-loop system, stability analysis and controller design criteria for MRFORC are developed.

A. Single-Rate Repetitive Control

Fig. 1 shows the typical closed-loop control system for a plug-in single-rate RC. The inner PI control loop includes $G_p(z)$, and $PI(z)$, which represent the transfer function of the control plant and the PI controller, respectively. The inherent unit delay of the digital implementation is modeled in the control plant. Besides, $R(z)$ is the reference input, $Y(z)$ is the output, $E(z) = R(z)-Y(z)$ is the tracking error, and $D(z)$ is the disturbance.

Transfer function of the RC shown in Fig. 1 can be expressed as

$$G_r(z)=\frac{U_r(z)}{E(z)}=\frac{z^{-N}}{1-Q(z)z^{-N}}S(z) \tag{1}$$

where $N = f_s / f$ with f being the fundamental frequency of $R(z)$ and/or $D(z)$, f_s being the sampling rate, and the order of RC is N. $U_r(z)$ is the output of RC, $S(z)$ is a compensation function to stabilize the overall closed-loop system, and $Q(z) = a_1z + a_0 + a_1z^{-1}$ with $2a_1 + a_0 = 1$ is a low-pass filter (LPF) to improve the robustness of the system [15].

If $Q(z) = 1$ and N is an integer, RC can provide zero steady-state error tracking of all harmonic components below the Nyquist frequency [23]. However, in an islanded microgrid (MG) the grid frequency f may be time-varying within a certain range [26]. Therefore, the order N would normally be fractional with a fixed sampling rate f_s. The conventional RC with the order N being the nearest integer to its real value cannot exactly track fractional period signals, since high control gains shift away from interested harmonic frequencies.

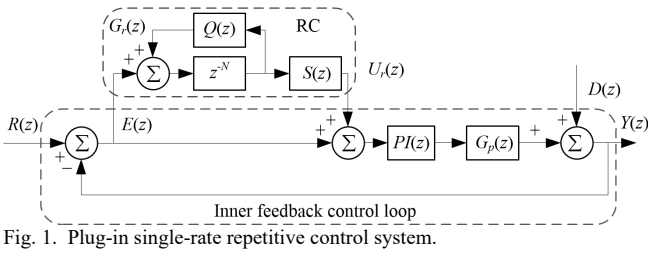

Fig. 1. Plug-in single-rate repetitive control system.

B. Single-Rate Fractional Order Repetitive Control

The fractional order repetitive control (FORC) scheme [31], which is based on the fractional delay filter design theory in digital signal processing [32] is suitable for both integer and non-integer period application. Fractional N can be divided into an integer part N_i = int[N] and a fractional part $F = N - N_i$. The transfer function of an ideal delay element for the fractional part can be written as

$$H_i(z)=z^{-F} \tag{2}$$

The above function can be approximated by a Lagrange interpolation polynomial FIR filter as follows [23], [25], [28].

$$z^{-F}\approx H(z)=\sum_{k=0}^{n}h(k)z^{-k} \tag{3}$$

where n is the order of FIR filter, and the coefficients $h(k)$ can be obtained as

$$h(k)=\prod_{i=0,i\neq k}^{n}\frac{F-i}{k-i} \tag{4}$$

Substituting (3) into (1), transfer function of FORC can be derived as

$$G_{fr}(z)=\frac{z^{-N_i}H(z)}{1-Q(z)H(z)z^{-N_i}}S(z) \tag{5}$$

When $F = 0$ the transfer function of FORC shown in (5) will be identical to that of RC shown in (1). FORC provides a general approach for tracking and/or eliminating of any periodic signal with arbitrary fundamental frequency. Its block diagram is shown in Fig. 2, where $G_r(z)$ in Fig. 1 is replaced by FORC $G_{fr}(z)$.

C. Multi-Rate Fractional-Order Repetitive Control

Fig. 3 shows the structure of the MRFORC system in z-domain, where $OP(z)$ represents the system z-domain open-loop transfer function for the inner PI control loop. It can be derived as (6). Note that the inner PI control loop has a feedback rate with a sampling period of $T_s = 1 / f_s$.

$$OP(z)=PI(z)G_p(z) \tag{6}$$

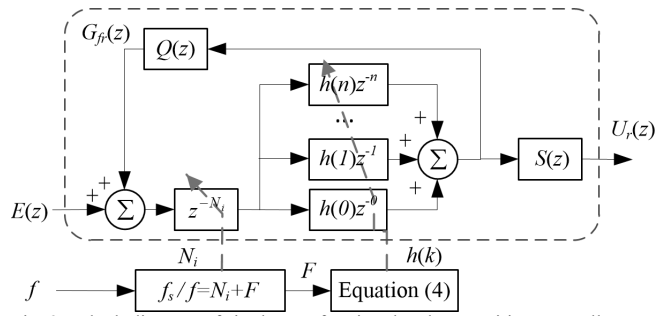

Fig. 2. Block diagram of single-rate fractional-order repetitive controller.

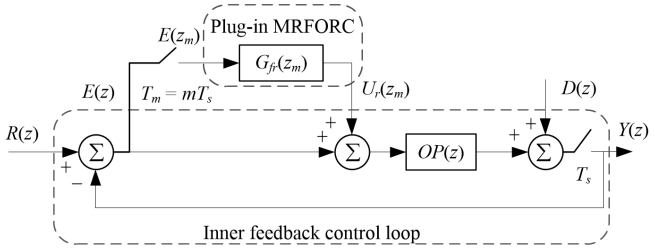

Fig. 3. The structure of the plug-in MRFORC system.

The MRFORC $G_{fr}(z_m)$ has a reduced feedback rate with a sampling period of $T_m = mT_s$, and m should be an integer. When m = 1, MRFORC becomes single-rate FORC. In the FORC block, $E(z_m)$ is the down-sampled error signal. And $U_r(z_m)$ is the output of FORC, which is interpolated by a zero order holder (ZOH). The relationship between the two sampling rates can be expressed as

$$T_m = mT_s, z = e^{sT_s}, z_m = z^m = e^{sT_m} \tag{7}$$

The transfer function of MRFORC $G_{fr}(z_m)$ can be derived from (5) as

$$G_{fr}(z_m) = \frac{U_r(z_m)}{E(z_m)} = \frac{z_m^{-N_i/m} H(z_m)}{1 - Q(z_m)H(z_m)z^{-N_i/m}} S(z_m) \tag{8}$$

C.1 Equivalent closed-loop system

To analyze the MRFORC system shown in Fig. 3, it is first transformed to an equivalent system with its sampling rate equals to the FORC rate. Block diagram of the equivalent system is shown in Fig. 4, where $\overline{OP}(z_m)$ represents the equivalent FORC rate open loop transfer function of inner PI control loop. Since only the closed loop transfer function will be used in FORC design, the equivalent closed loop transfer function of inner PI control loop will be developed hereafter.

On the basis of the open-loop transfer function for the inner PI control loop (6), the closed-loop transfer function of inner feedback control loop can be expressed as

$$CP(z) = OP(z)/[1 + OP(z)] \tag{9}$$

Then, $CP(z)$ can be rewritten in the state-space form as follows.

$$\begin{cases} x_f(k+1) = A_f x_f(k) + B_f u_f(k) \\ y_f(k) = C_f x_f(k) + D_f v_f(k) \end{cases} \tag{10}$$

where x_f, u_f, y_f, and v_f are the state variables, input, output, and disturbance, respectively, k denotes discrete time index with sampling period T_s.

Since the FORC rate is m times slower than the inner feedback loop rate, the FORC will use the previous 'm' outputs and the current input to produce an output at the current time instant. Denotes the discrete time index corresponding to the

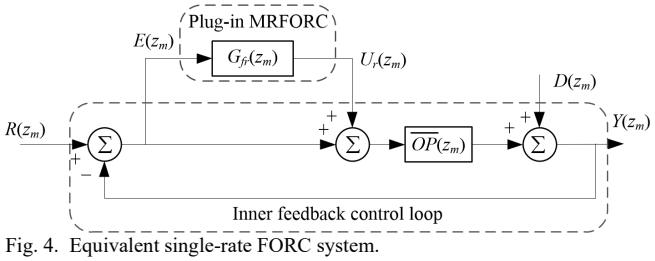

Fig. 4. Equivalent single-rate FORC system.

FORC rate by K. For (10), $k = mK + i$ (i = 1,2, . . . m), the state equations in an FORC rate are [30], [29].

$$\begin{cases} x_f(mK+1) = A_f x_f(mK) + B_f u_f(mK) \\ x_f(mK+2) = A_f x_f(mK+1) + B_f u_f(mK) \\ \vdots \\ x_f(mK+m) = A_f x_f(mK+m-1) + B_f u_f(mK) \end{cases} \tag{11}$$

Then, by down-sampling, its slow-rate state equation is

$$\begin{cases} x_s(K+1) = A_s x_s(K) + B_s u_s(K) \\ y_s(K) = C_s x_s(K) + D_s v_s(K) \end{cases} \tag{12}$$

where $A_S = A_f^m$, $B_S = (A_f^{m-1}B_f + A_f^{m-2}B_f + \cdots + A_fB_f + B_f)$, $C_s = C_f$ and $D_s = D_f$. The equivalent FORC rate closed loop transfer function of inner PI control loop is

$$\overline{CP}(z_m) = C_s(z_m I - A_s)^{-1} B_s \tag{13}$$

C.2 Stability analysis

According to Fig.4, the error of the overall system can be derived as

$$\overline{E}(z_m) = \frac{1 - Q(z_m)H(z_m)z_m^{-N_i/m}}{1 - z_m^{-N_i/m}H(z_m)[Q(z_m) - S(z_m)\overline{CP}(z_m)]} \cdot \frac{1}{1 + \overline{OP}(z_m)} \times [R(z_m) - D(z_m)] \tag{14}$$

With further manipulation on (14), the tracking error dynamics is expressed as

$$\overline{E}(z_m) = \overline{E}(z_m) z_m^{-N_i/m} [Q(z_m) - S(z_m)\overline{CP}(z_m)] \frac{H(z_m)}{1 + \overline{OP}(z_m)} + \frac{1 - Q(z_m)H(z_m)z_m^{-N_i/m}}{1 + \overline{OP}(z_m)} \times [R(z_m) - D(z_m)] \tag{15}$$

Assuming $T(z_m) = Q(z_m) - S(z_m)\overline{CP}(z_m)$, it can be observed that the tracking error $\overline{E}(z_m)$ is bounded if

$$\left| T(e^{j\omega T_m}) \right|_{z_m = e^{j\omega T_m}} = \left| Q(e^{j\omega T_m}) - S(e^{j\omega T_m})\overline{CP}(e^{j\omega T_m}) \right| < 1 < \frac{\left| [1 + \overline{OP}(e^{j\omega T_m})] \right|}{\left| H(e^{j\omega T_m}) \right|}, \tag{16}$$

where $\omega \in (0, \pi/T_m)$, and π/T_m is the Nyquist frequency.

The stability criteria can be interpreted geometrically [33] as shown in Fig. 5. The arrowed lines shown in Fig. 5 represent the vectors for $Q(e^{j\omega T_m})$, $S(e^{j\omega T_m})\overline{CP}(e^{j\omega T_m})$ and $T(e^{j\omega T_m})$ at a specific frequency, respectively. In fact, the vectors for $Q(e^{j\omega T_m})$ and $S(e^{j\omega T_m})\overline{CP}(e^{j\omega T_m})$ should start from (0, 0). However, for the convenience of stability analysis and parameter design criteria developing, the ends of the vectors for both $Q(e^{j\omega T_m})$ is fixed at (1, 0), the other vectors are moved along the real axis, such that the readability of the figure can be improved. Note that the relationship among the vectors remains unchanged. In case that the vector for $T(e^{j\omega T_m})$ never goes out the unity circle centred at (1, 0) in the whole angular frequency range, the stability condition is held , which is shown in Fig. 5(a). By contrast, Fig. 5(b) represents an unstable case, in which the vector for $T(e^{j\omega T_m})$ goes out of unit circle at high frequencies. The trajectory of the vector for $T(e^{j\omega T_m})$ with ω

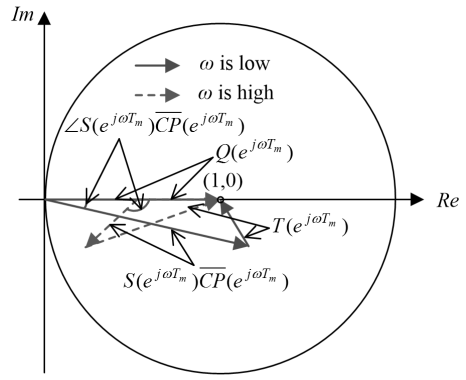

(a) Stable condition

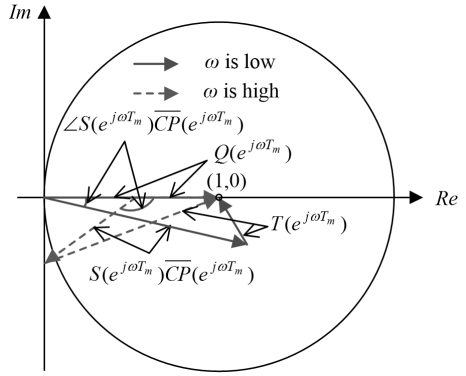

(b) Unstable condition

Fig. 5. Geometric illustration of the sufficient condition of stability.

increasing from zero to the Nyquist frequency represents Nyquist curve of $T(z_m)$. Thus, the system stability is guaranteed only when the Nyquist curve of $T(z_m)$ does not exceeds the unity circle.

It can be inferred from Fig. 5 that with the same magnitude of $S(e^{j\omega T_m})\overline{CP}(e^{j\omega T_m})$, the larger phase lag of it makes vectors for $T(e^{j\omega T_m})$ more easily to go out of the unit circle, therefore one parameter design criteria for FORC is to try to keep $S(e^{j\omega T_m})\overline{CP}(e^{j\omega T_m})$ with small phase lag at low and middle frequency range.

C.3 Design of $S(z_m)$

Considering that steady-state tracking error is another key criterion to evaluate a controller's performance, it is derived in (17) by simplifying (14). Note that in steady-state the tracking error is periodic and $z_m^{-N_i/m}H(z_m) \approx 1$.

$$\left|\overline{E}(e^{j\omega T_m})\right| \approx \overbrace{\left|\frac{1-Q(e^{j\omega T_m})H(e^{j\omega T_m})}{1-Q(e^{j\omega T_m})+S(e^{j\omega T_m})\overline{CP}(e^{j\omega T_m})}\right|}^{|E_1(e^{j\omega T_m})|} \times \overbrace{\left|\frac{R(e^{j\omega T_m})-D(e^{j\omega T_m})}{1+\overline{OP}(e^{j\omega T_m})}\right|}^{|E_2(e^{j\omega T_m})|}. \quad (17).$$

where $\left|E_2(e^{j\omega T_m})\right|$ represents the steady-state error for reference tracking and disturbance rejection with the inner PI control loop. It can be seen from (17) that the system steady-state error with MRFORC embedded becomes $\left|E_1(e^{j\omega T_m})\right|$ times smaller, compared with that of the PI controlled system. Magnitude of $\left|E_1(e^{j\omega T_m})\right|$ indicates the harmonic rejection capability of the MRFORC, i.e., $\left|Q(e^{j\omega T_m})\right|$ close to 1 and/or large $S(e^{j\omega T_m})\overline{CP}(e^{j\omega T_m})$ can ensure small error. Thus, another parameter design criteria for MRFORC is to try to keep $S(e^{j\omega T_m})\overline{CP}(e^{j\omega T_m})$ with enough magnitude at low and middle frequency range.

As illustrated in C.2, small phase lag of $S(e^{j\omega T_m})\overline{CP}(e^{j\omega T_m})$ makes the system to have larger stability margin, i.e., to achieve the same stability margin, $S(e^{j\omega T_m})\overline{CP}(e^{j\omega T_m})$ with small phase lag can have larger magnitude. $S(z_m)$ can be chosen as inverse of the closed-loop system transfer function $1/\overline{CP}(z_m)$ [15], which leads to perfect phase lag compensation. However, it makes $S(z_m)$ exhibits as a high-pass filter, which may amplify the high frequency component, and therefore worsen the system stability. An alternative way is choosing $S(z_m)$ with the following form[16]:

$$S(z_m) = K_r \cdot F_2(z_m) \cdot z_m^d \quad (18)$$

where, K_r is the FORC gain, $F_2(z_m)$ is a second-order digital filter and z_m^d is a pure leading element. $F_2(z_m)$ is used to depress the gain in high frequency range for enhancing the stability, and z_m^d is used to compensate the delay of $F_2(z_m)$ as well as $\overline{CP}(z_m)$.

III. Case Design

To evaluate the performance of the proposed MRFORC scheme for APF, a three-phase compact islanded MG test bed is built in the laboratory and the corresponding block diagram is shown in Fig. 6. The experimental test bed consists of two converters connected to a common AC bus through LCL filters. One of them serves as grid forming inverter while the other one

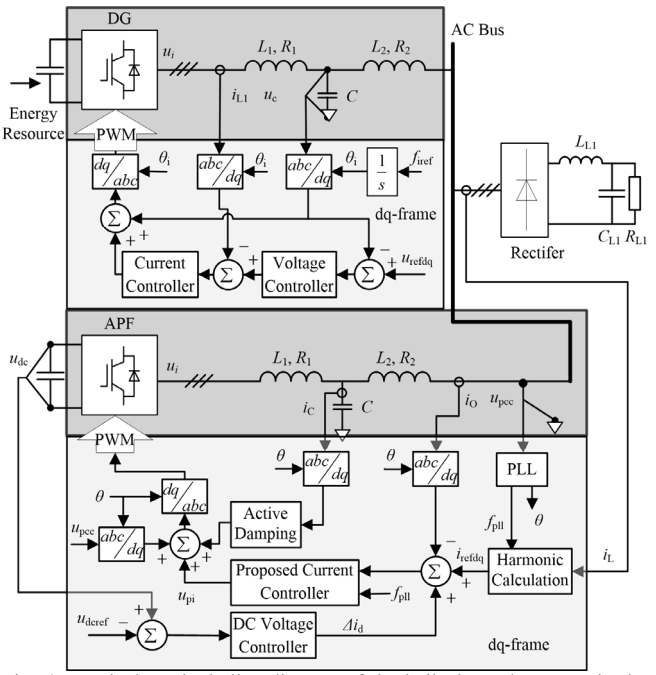

Fig. 6. Equivalent single-line diagram of the built three-phase MG in the laboratory.

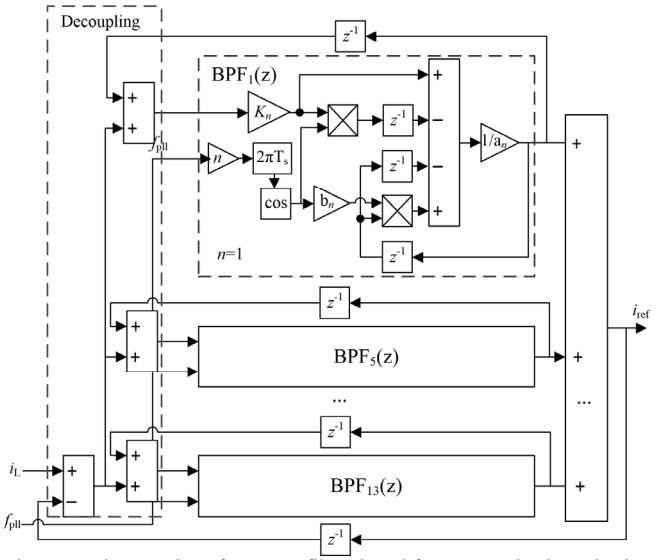

Fig. 7. Implementation of resonant filters based frequency adaptive selective harmonic detection.

acts as APF with the proposed MRFORC scheme implemented in *dq*-frame. The control of APF includes phase locked loop (PLL), harmonic calculation, DC voltage control, current control and active damping.

An array of resonant filters [34], [35] is utilized to selectively extract the harmonic components of load current, since selective harmonic compensation strategy brings many advantages, such as reduction of the filter rating and the current-control bandwidth, less possibility of dangerous interactions with system resonances [9]. In addition, to improve the frequency adaptability of the resonant filters, the central frequencies of each resonant filter is online calculated by using a PLL [36] with bandwidth equal to 62.8 rad/s. Moreover, to further enhance the harmonic detection accuracy, the interference among each harmonics was canceled by adding a decoupling loop, in which the irrelevant fundamental/harmonic component is subtracted before being fed to the relevant resonant filter. The implementation of resonant filters based frequency adaptive selective harmonic detection block is illustrated in Fig. 7, where the transfer function of resonant filter can be expressed in *z*-domain as.

$$BPF_n(z) = \frac{K_n[z^2 - \cos(2\pi T_s f_{pll} n)z]}{a_n z^2 - b_n \cos(2\pi T_s f_{pll} n)z + 1)}. \quad (19)$$

where $K_n = K_{in}T_s$, $a_n = 1 + K_n$, and $b_n = 2 + K_n$, K_n is the integral coefficient, T_s is the sampling period and n represents harmonic order.

Fig.8 shows the experimental setup. Two 2.2-kW Danfoss inverters are adopted as grid forming converter and APF, respectively. The control algorithm is applied by using a DS1006 dSPACE system with a 10-kHz sampling frequency. The power stage parameters are illustrated in Table I. Based on these parameters and design criteria derived in the above section, the controller will be elaborately designed hereafter. It should be mentioned that the study case is on the basis of the built three-phase MG in the laboratory. However, the power stage parameters of the built three-phase MG are not

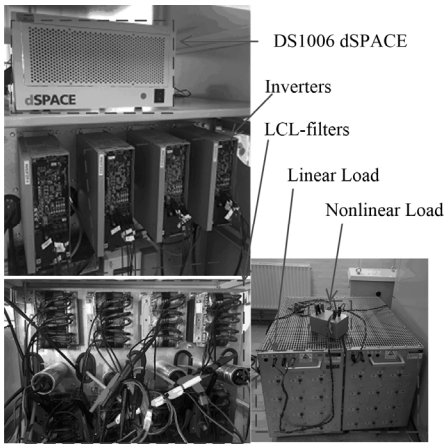

Fig. 8. Hardware picture for the inverters and the control platform.

TABLE I
CIRCUIT PARAMETERS

	Symbol	Quantity	Value
Inverters	L_1	Converter side inductor	1.8mH
	R_1	parasitic resistance of L_1	0.2Ω
	L_2	Grid side inductor	1.8mH
	R_2	parasitic resistance of L_1	0.2Ω
	C	Capacitor of LCL-filter	27uF
Linear load	R_{L2}	Load resistance	115Ω
Nonlinear load	L_{L1}	DC-link inductor	100uH
	C_{L1}	DC-link Capacitor	235uF
	R_{L1}	Load resistance	115Ω

specialized for APF, the resonance frequency of LCL filter is about 1 kHz, which should be commonly designed larger than 3 kHz in APF applications [8]–[13]. The value of main circuit parameters limits the bandwidth of current loop, and thus only dominating harmonic components (5^{th}, 7^{th}, 11^{th}, 13^{th}) of the nonlinear load can be selectively compensated here in the experiment to verify the proposed control scheme.

A. Model of control plant and active damping compensator

By neglecting the parasitic parameters of the LCL filter of the APF system depicted in Fig. 6, the power plant model is illustrated in Fig. 9, then the *s*-domain transfer function from inverter output voltage U_I to grid side inductor current I_o is shown in (20). Note that capacitor-current-feedback based active damping [37], [38] is adopted to stabilized the system.

$$G_p(s) = \frac{I_o(s)}{U_I(s)} = \frac{1}{L_1 L_2 C s} \cdot \frac{1}{(s^2 + 2\xi\omega_{res} s + \omega_{res}{}^2)} \quad (20)$$

where $\omega_{res} = \sqrt{(L_1 + L_2)/(L_1 L_2 C)}$, $\xi = K_D / [2\sqrt{L_1(L_1 + L_2)/(L_2 C)}]$,

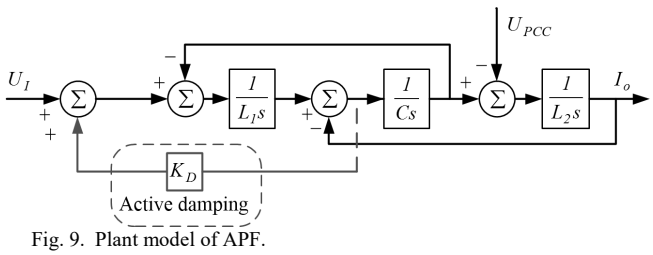

Fig. 9. Plant model of APF.

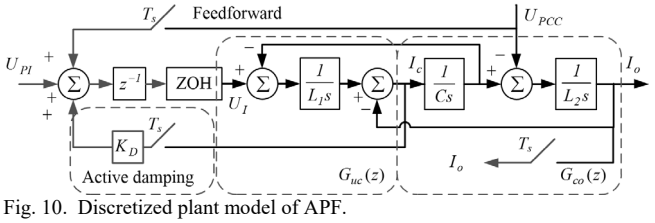

Fig. 10. Discretized plant model of APF.

K_D denotes the gain along capacitor-current-feedback path. In this study, ξ is set to 0.4, then $K_D = 9$.

To accurately derive the z-domain transfer function of the plant of APF for further MRFORC parameters design, both the sampling delay and the inherent unit delay of the digital controller were considered. The discretized plant of APF was shown in Fig. 10, where, z^{-1} represents the unit delay and zero-order holder (ZOH) stands for the sampling delay. The equivalent z-domain transfer function of the plant, which is from PI output U_{PI} to grid side inductor current I_o, can be regarded as two cascaded parts: from converter output voltage to capacitor current and from capacitor current to grid current. The corresponding z-domain transfer functions were given in (21) and (22). It is worth noting that (21) is discretized from its s-domain transfer function with ZOH transformation, while (22) with impulse-invariant (IMP) transformation. More detail can be found in [39].

$$G_{uc}(z) = \frac{I_c(z)}{U_I(z)} = \frac{\sin(\omega_{res}T_s)}{L_1} \cdot \frac{z-1}{z^2 - 2z\cos(\omega_{res}T_s) + 1} \tag{21}$$

$$G_{co}(z) = \frac{I_o(z)}{I_c(z)} = \frac{T_s^2 z}{L_2 C(z-1)^2} \tag{22}$$

Based on (21) and (22), the equivalent z-domain transfer function of the plant can be derived as

$$G_p(z) = \frac{I_o(z)}{U_{PI}(z)} = \frac{z^{-1}G_{uc}(z)G_{co}(z)}{1 + z^{-1}K_D G_{uc}(z)} \tag{23}$$

Substituting the parameters illustrated in Table I in to (23), $G_p(z)$ can be derived as

$$G_p(z) = \frac{0.0107\,z}{z^4 - 2.6024\,z^3 + 3.0811\,z^2 - 1.9574\,z + 0.4787}. \tag{24}$$

B. B. Inner PI control parameter design

The PI controller was designed by approximate the LCL filter as a L filter [40], then the PI controller gains can be set as follows:

$$PI(s) = K_p\left(1 + \frac{1}{T_i s}\right) \tag{25}$$

$$T_i = (L_1 + L_2)/(R_1 + R_2) \tag{26}$$

$$K_p = \omega_c(L_1 + L_2) \tag{27}$$

where ω_c is the crossover angular frequency. Set ω_c = 1570 rad/s, then K_p = 5.65 and T_i = 0.018. Applying Tustin transformation to (25), $PI(z)$ in z-domain can be obtained. Then substituting $PI(z)$ into (6) and (9), the system open-loop and closed-loop transfer functions can be obtained in z-domain . Bode plots of the open-loop and closed-loop system transfer functions $OP(z)$ and $CP(z)$ are given in Fig. 11. It can be concluded from the figure that although the inner PI control loop is very robust due to large phase margin of 90º, the harmonic tracking ability is very limited because of large phase lag of $CP(z)$ at high frequencies, e.g. 90º phase lag at 500 Hz. In order to enhance harmonic tracking capability, the MRFORC is added.

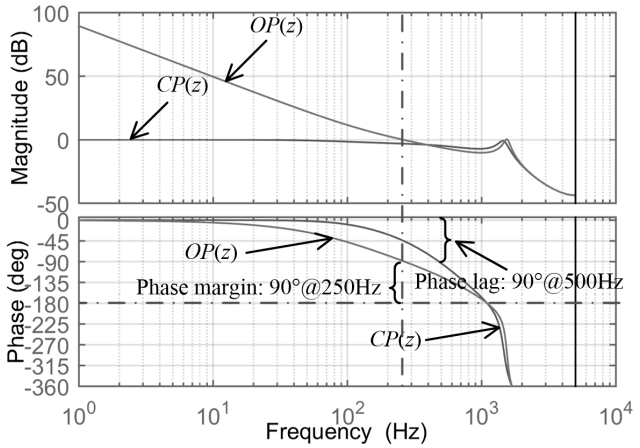

Fig. 11. Bode plots of open-loop and closed-loop transfer functions.

C. C. MRFORC parameters design

Before design the parameters of $S(z_m)$, the equivalent closed loop transfer function $\overline{CP}(z)$ with different sampling rates (m = 1, 2, 4) for the above $CP(z)$ were developed. Firstly, the before transfer function $CP(z)$ was transferred into states equation in MATLAB. Afterwards, (12) can be used to calculate the equivalent FORC rate closed-loop system states equations. Finally, the state equations were transferred back to transfer function for MRFORC parameter design. Bode plot of the equivalent closed loop transfer function $\overline{CP}(z)$ with different sampling rates were illustrated in Fig. 12, where the magnitude characteristics are almost the same for m = 1, 2, 4 at all frequency range, while the phase characteristics only overlapped at frequencies lower than 100 Hz. For frequencies higher than 100 Hz, the phase lag will increase as the sampling rate decrease (bigger m value). Thus, the compensation function $S(z_m)$ should be separately designed by take this phase lag into consideration.

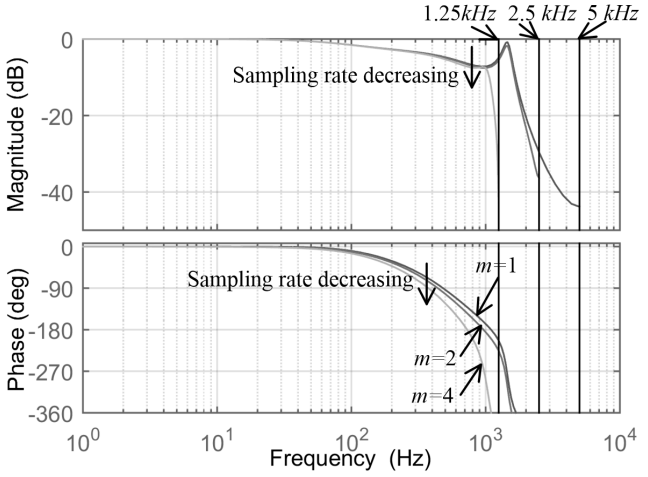

Fig. 12. Bode plots of equivalent closed loop transfer function with different sampling rates.

According to (18), $S(z_m)$ concludes a FORC gain, a second-order filter and a pure leading element. Note that the FORC gain ranges from 0 to 2 theoretically [15]. A larger value of the FORC gain means higher tracking precision with smaller stability margin and vice versa. The second-order filter and leading element is usually tuned by using trial and error method [16]. The tuned $S(z_m)$ is given in (28), where the angular frequency of the second-order digital filter is set to 15625 rad/s and damping ratio is set to 0.707 for all m values (m=1, 2, 4), while the orders of leading elements are set to 6, 3 and 2 for different m equlas to 1, 2, and 4, respectively.

$$S(z_m)=\begin{cases} k_r \cdot z_m^6 \dfrac{0.2261z_m^2+0.4523z_m+0.2262}{z_m^2-0.2810z_m+0.1856}, m=1 \\ k_r \cdot z_m^3 \dfrac{0.4338z_m^2+0.8675z_m+0.4338}{z_m^2+0.5159z_m+0.2191}, m=2 \\ k_r \cdot z_m^2 \dfrac{0.6446z_m^2+1.2891z_m+0.6446}{z_m^2+1.1585z_m+0.4198}, m=4 \end{cases} \quad (28)$$

Fig. 13 illustrates Bode phase plot of $S(z_m)\overline{CP}(z_m)$ at different FORC sampling rates. It can be seen from Fig. 13 that $S(z_m)$ compensates the phase delay of $\overline{CP}(z_m)$ for different m values, which complied well with the design guide. At frequencies below 100Hz, the phase characteristic of $S(z_m)\overline{CP}(z_m)$ for all m values are the same, which implies the same control performance at low frequencies. However, the phase characteristic deviates with each other at frequencies above 100Hz. For the system with m =1, its phase response is more approaching zero, which implies it has the best harmonic reference tracking capability among the three systems. Meanwhile, for system with m =4, lowest harmonic reference tracking performance is obtained, since it has the largest phase deviation.

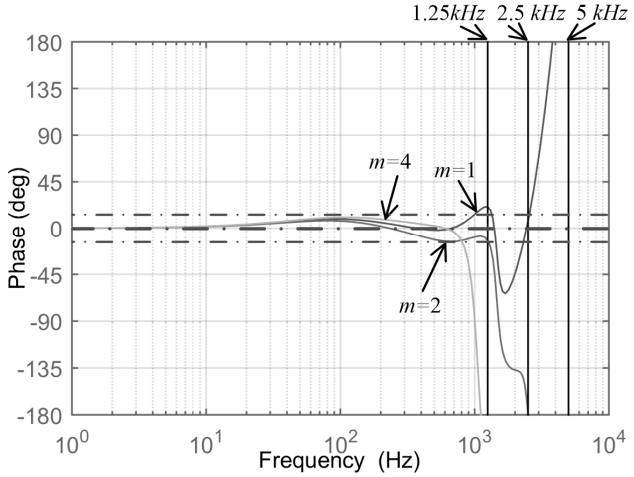

Fig. 13. Phase-frequency response characteristic curves of $S(z_m)\overline{CP}(z_m)$ with different m values.

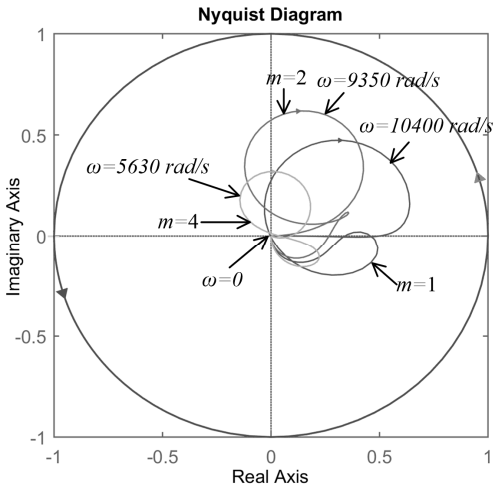

Fig. 14. Nyquist curves of $T(e^{j\omega T_m})$ with different m values.

Fig. 14 illustrates the Nyquist curves of $T(e^{j\omega T_m})$ with different m values when k_r equals to 1. The Nyquist curves are all inside the unit circle, thus the system stability is guaranteed for all m values.

IV. Experimental Results

To verify the feasibility of multi-rate scheme and the frequency adaptability of MRFORC, the control algorithms are programmed in Matlab/Simulink and compiled to a dSPACE controller board (DS1006) to control both grid forming converter and APF. The experimental data are all saved by dSPACE ControlDesk and then plotted in Matlab.

A. Current reference tracking performance at different FORC sampling rate

The evidence of the MRFORC scheme is first given in Fig. 15. It can be seen from the figure that the MRFORC need to be implemented at every sampling cycle when m=1 (sampling rate of MRFORC equals to 10 kHz), while it only needs to be executed once in two/four sampling cycles when m=2/4 (sampling rate of FORC reduced to 5 kHz/2.5kHz). It also can be seen that the FORC output signals are updated with the interleaved mode under dq-frame because of the interleaved conducting of FORC, consequently, the computation burden is reduced per sampling cycle. And the memory space needed for fundamental period delay element in FORC is also reduced to 50% and 25% for m=2, and 4, respectively.

Fig. 16 illustrates the steady-state current tracking performance with different FORC sampling rate. In Fig. 16,

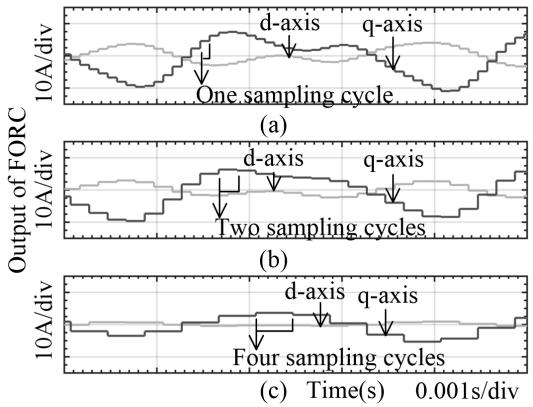

Fig. 15. Waveforms of FORC output signals at different sampling rate. (a) m=1, (b) m=2, (c) m=4

load and grid currents, current reference, output current and tacking error of APF are presented. As shown in the figure, when m = 1 the peak value of the tracking error is about 0.27A and relative error to current reference (about 6A) is around 4.5%. When m = 2, the peak value of current tracking error is increases to about 0.77A and relative error to current reference (about 6A) is around 12.8%. And when m = 4, the peak value of current reference tracking error is enlarged to about 1.3A and relative error to current reference (about 4.5A) is around 28.9%. It can also been seen that the smaller current reference tracking error the better harmonic compensation performance. It can be concluded from above that the benefit of multi-rate scheme is achieved at the expense of performance degradation, which agrees with the theoretical analysis presented in section III C.

The tradeoff between the performance degradation and sampling rate reduction should be made depending on the requirement in different applications. For the system with higher control/switching frequency, it may have a faster inner feedback PI loop with less digital system delay. However, higher execution frequency is not necessary for the FORC aimed at improving the steady-state performance. Considering that the system with higher control/switching frequency has shorter interruption time, the importance of the multi-rate technique in saving computation time becomes more meaningful. FORC loop with 5kHz execution frequency may have similar steady state performance with that of a system with 10 kHz or 20 kHz control/switching frequency. Meanwhile, FORC only need to be implemented once in two/four control cycles with 10 kHz or 20 kHz control/switching frequency, thus computation time is significantly reduced.

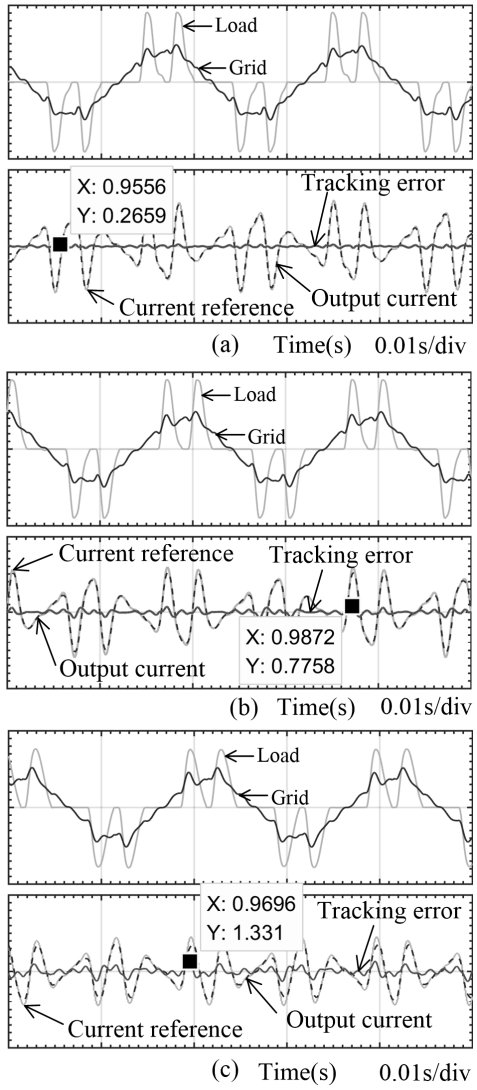

Fig. 16. Steady-state current reference tracking performance with different FORC sampling rate. (a) m = 1, (b) m = 2, (c) m = 4

B. Current reference tracking performance under wide grid frequency variation (m = 2)

To evaluate the frequency adaptivity of the MRFORC, experiments are carried out with the FORC sampling rate equals to 5 kHz (m = 2). Fig. 17 illustrates the steady-state current reference tracking performance at different grid frequencies. The current reference tracking error is about 0.75 A at grid frequency equals to 55 Hz and 0.73 A at 45Hz, as shown in Fig. 17 (a) and (b), respectively. Although the approximation accuracy of the FIR filter in the FORC for the ideal fractional delay element was changed along with the variation of grid frequency, which may has an effect on current reference tracking performance, the effect is really small and often has been neglected [23].

Fig. 18 shows the transient response of current tracking error during grid frequency steps. It should be noted that the grid frequency is obtained from PLL. Fig. 18(a) illustrates the waveforms when grid frequency steps up from 50 Hz to 55 Hz, while Fig. 18(b) depicts the waveforms of grid frequency steps down from 50Hz to 45Hz. The regulation time is about 0.15s and 0.05s for grid frequency step up and step down, respectively. The dynamic error for frequency step up is smaller than the one for frequency step down. This difference is likely depended on the difference of the change in the internal mode of the MRFORC during grid frequency step up and step down process. The relationship of the internal mode to the MFORC is similar with that of the integrator to the PI controller. It takes more responsibility for zero steady-state error tracking and determining dynamic regulation time. Although the existence of different response time, it can be concluded that

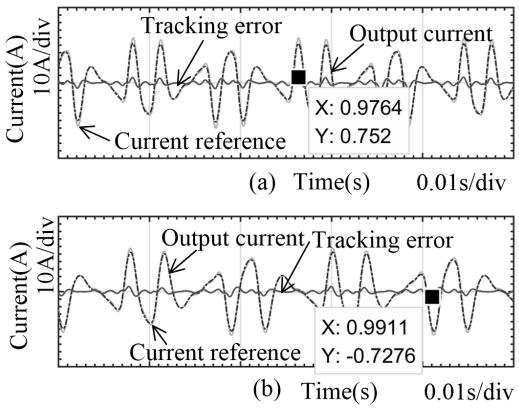

Fig. 17. Steady-state current reference tracking error under different grid frequency. (a) 55Hz, (b) 45Hz

the proposed MRFORC has good frequency adaptivity.

C. Performance evaluation for APF with MRFOC

Steady-state current waveforms of the APF and its frequency spectrum are illustrated in Fig. 19 to evaluate the steady performance of APF with MRFORC. In Fig. 19 (a), from up to bottom are 'Load current', 'APF output current', and 'Grid current', respectively. Fig. 19 (b) illustrates the frequency spectrums of load and grid currents. As mentioned in Section III, due to the limit of the main circuit parameters, only dominating harmonic components of the nonlinear load have been considered and selectively compensated. It can be seen that the high order harmonics of load current are really small, and dominant harmonics are low order harmonics, which have been greatly reduced.

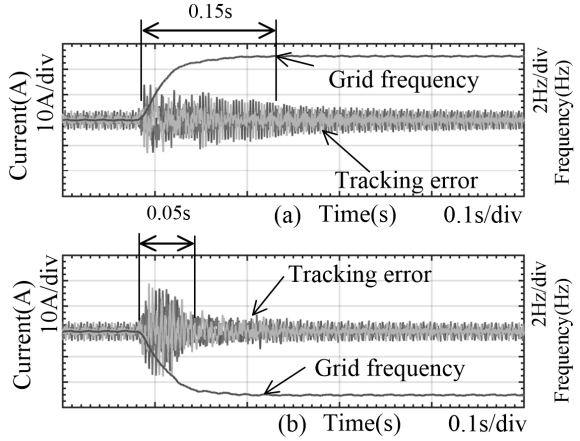

Fig. 18. Current reference tracking error during step changes of grid frequency. (a) 50Hz->55Hz, (b)50Hz->45Hz

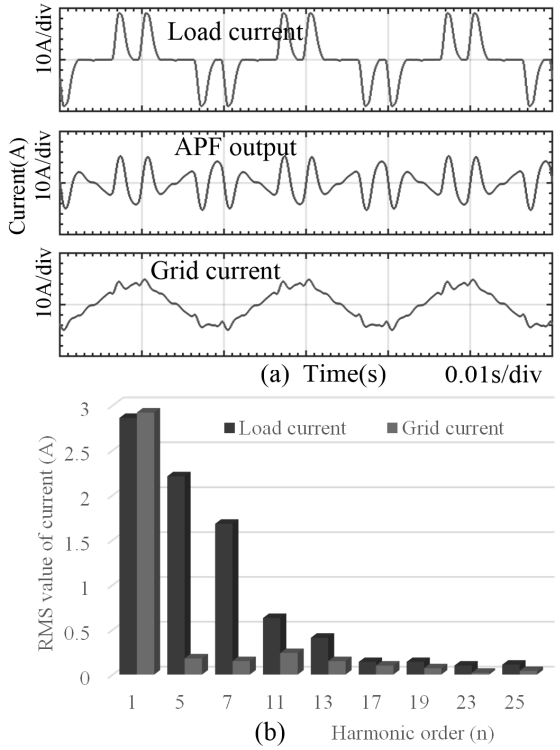

Fig. 19. (a) Steady-state experimental waveforms of MRFORC control and (b) frequency spectrums of load and grid currents.

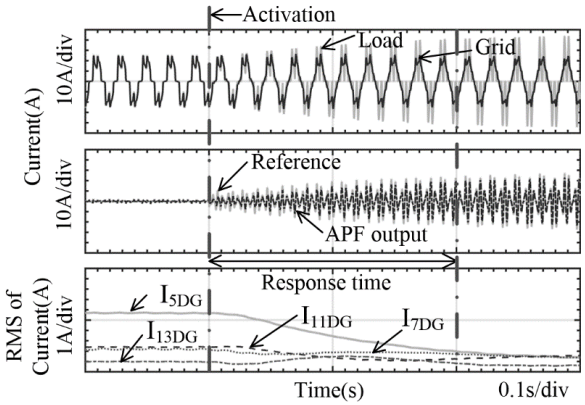

Fig. 20. Transient experimental waveforms of MRFORC control APF.

The transient current waveforms of the APF are illustrated in Fig. 20 to evaluate the dynamic performance of MRFORC. From up to bottom are 'Load and grid currents', 'Reference and APF output currents', and 'Residual dominant harmonics (5^{th}, 7^{th}, 11^{th}, 13^{th}) in grid current', respectively. It can be seen that before APF activation grid side current is distorted by the nonlinear load, while after that, the selected main harmonic current components of load are compensated, consequently, the harmonic distortion of grid side current is reduced obviously. Note that it takes about 0.2s for the APF to reach the steady-state.

V. Conclusion

This paper proposes a MRFORC scheme for a three-phase shunt APF. The synthesis, stability analysis and parameters tuning criteria of the MRFORC system are given in detail. The MRFORC is able to provide high tracking accuracy for harmonic reference even in the presence of wide grid frequency variations. It has also been demonstrated that both the computational burden and the memory space are reduced at the cost of the performance degradation to some extent. The laboratory tests of a compact island three-phase MG are carried out to validate the feasibility and effectiveness of the proposed scheme. Besides, the proposed approach is not only suitable for APF, but also can be applied in distributed generation (DG) inverters for the purpose of providing harmonic compensation functions to realize a cost-effective and flexible operation of DG units.

References

[1] H. Akagi, "New trends in active filters for power conditioning," *Ind. Appl. IEEE Trans. On*, vol. 32, no. 6, pp. 1312–1322, 1996.

[2] H. Akagi, "Active Harmonic Filters," *Proc. IEEE*, vol. 93, no. 12, pp. 2128–2141, Dec. 2005.

[3] S. Buso, S. Fasolo, L. Malesani, and P. Mattavelli, "A dead-beat adaptive hysteresis current control," *Ind. Appl. IEEE Trans. On*, vol. 36, no. 4, pp. 1174–1180, 2000.

[4] S. Buso, L. Malesani, and P. Mattavelli, "Comparison of current control techniques for active filter applications," *Ind. Electron. IEEE Trans. On*, vol. 45, no. 5, pp. 722–729, 1998.

[5] D. N. Zmood, D. G. Holmes, and G. H. Bode, "Frequency-domain analysis of three-phase linear current regulators," *Ind. Appl. IEEE Trans. On*, vol. 37, no. 2, pp. 601–610, 2001.

[6] X. Yuan, W. Merk, H. Stemmler, and J. Allmeling, "Stationary-frame generalized integrators for current control of active power filters with

zero steady-state error for current harmonics of concern under unbalanced and distorted operating conditions," *Ind. Appl. IEEE Trans. On*, vol. 38, no. 2, pp. 523–532, 2002.
[7] R. I. Bojoi, G. Griva, V. Bostan, M. Guerriero, F. Farina, and F. Profumo, "Current Control Strategy for Power Conditioners Using Sinusoidal Signal Integrators in Synchronous Reference Frame," *IEEE Trans. Power Electron.*, vol. 20, no. 6, pp. 1402–1412, Nov. 2005.
[8] C. Lascu, L. Asiminoaei, I. Boldea, and F. Blaabjerg, "High Performance Current Controller for Selective Harmonic Compensation in Active Power Filters," *IEEE Trans. Power Electron.*, vol. 22, no. 5, pp. 1826–1835, Sep. 2007.
[9] J. Miret, M. Castilla, J. Matas, J. M. Guerrero, and J. C. Vasquez, "Selective Harmonic-Compensation Control for Single-Phase Active Power Filter With High Harmonic Rejection," *IEEE Trans. Ind. Electron.*, vol. 56, no. 8, pp. 3117–3127, Aug. 2009.
[10] L. Malesani, P. Mattavelli, and S. Buso, "Robust dead-beat current control for PWM rectifiers and active filters," *IEEE Trans. Ind. Appl.*, vol. 35, no. 3, pp. 613–620, May 1999.
[11] Yang Han, Lin Xu, M. M. Khan, Chen Chen, Gang Yao, and Li-Dan Zhou, "Robust Deadbeat Control Scheme for a Hybrid APF With Resetting Filter and ADALINE-Based Harmonic Estimation Algorithm," *IEEE Trans. Ind. Electron.*, vol. 58, no. 9, pp. 3893–3904, Sep. 2011.
[12] A. Garcia-Cerrada, O. Pinzon-Ardila, V. Feliu-Batlle, P. Roncero-Sanchez, and P. Garcia-Gonzalez, "Application of a Repetitive Controller for a Three-Phase Active Power Filter," *IEEE Trans. Power Electron.*, vol. 22, no. 1, pp. 237–246, Jan. 2007.
[13] A. G. Yepes, F. D. Freijedo, O. Lopez, and J. Doval-Gandoy, "High-Performance Digital Resonant Controllers Implemented With Two Integrators," *IEEE Trans. Power Electron.*, vol. 26, no. 2, pp. 563–576, Feb. 2011.
[14] B. Francis and W. Wonham, "The internal model principle for linear multivariable regulators," *Applied Mathematics and Optimization*, vol. 2, no. 2, pp. 170–194, 1975.
[15] Keliang Zhou and Danwei Wang, "Digital repetitive controlled three-phase PWM rectifier," *IEEE Trans. Power Electron.*, vol. 18, no. 1, pp. 309–316, Jan. 2003.
[16] Kai Zhang, Yong Kang, Jian Xiong, and Jian Chen, "Direct repetitive control of SPWM inverter for UPS purpose," *IEEE Trans. Power Electron.*, vol. 18, no. 3, pp. 784–792, May 2003.
[17] P. Mattavelli and F. P. Marafao, "Repetitive-Based Control for Selective Harmonic Compensation in Active Power Filters," *IEEE Trans. Ind. Electron.*, vol. 51, no. 5, pp. 1018–1024, Oct. 2004.
[18] W. Lu, K. Zhou, and D. Wang, "General parallel structure digital repetitive control," *Int. J. Control*, vol. 86, no. 1, pp. 70–83, Jan. 2013.
[19] T. Hornik and Q.-C. Zhong, "H∞ repetitive voltage control of grid-connected inverters with a frequency adaptive mechanism," *IET Power Electron.*, vol. 3, no. 6, p. 925, 2010.
[20] D. Chen, J. Zhang, and Z. Qian, "An Improved Repetitive Control Scheme for Grid-Connected Inverter With Frequency-Adaptive Capability," *IEEE Trans. Ind. Electron.*, vol. 60, no. 2, pp. 814–823, Feb. 2013.
[21] J. M. Olm, G. A. Ramos, and R. Costa-Castelló, "Stability analysis of digital repetitive control systems under time-varying sampling period," *IET Control Theory Appl.*, vol. 5, no. 1, p. 29, 2011.
[22] E. Kurniawan, Z. Cao, and Z. Man, "Design of Robust Repetitive Control With Time-Varying Sampling Periods," *IEEE Trans. Ind. Electron.*, vol. 61, no. 6, pp. 2834–2841, Jun. 2014.
[23] Z.-X. Zou, K. Zhou, Z. Wang, and M. Cheng, "Frequency-Adaptive Fractional-Order Repetitive Control of Shunt Active Power Filters," *IEEE Trans. Ind. Electron.*, vol. 62, no. 3, pp. 1659–1668, Mar. 2015.
[24] T. Liu and D. Wang, "Parallel Structure Fractional Repetitive Control for PWM Inverters," *IEEE Trans. Ind. Electron.*, vol. PP, no. 99, pp. 1–1, 2015.
[25] Y. Yang, K. Zhou, H. Wang, F. Blaabjerg, D. Wang, and B. Zhang, "Frequency Adaptive Selective Harmonic Control for Grid-Connected Inverters," *IEEE Trans. Power Electron.*, vol. 30, no. 7, pp. 3912–3924, Jul. 2015.
[26] J. C. Vasquez, J. M. Guerrero, M. Savaghebi, J. Eloy-Garcia, and R. Teodorescu, "Modeling, Analysis, and Design of Stationary-Reference-Frame Droop-Controlled Parallel Three-Phase Voltage Source Inverters," *IEEE Trans. Ind. Electron.*, vol. 60, no. 4, pp. 1271–1280, Apr. 2013.
[27] R. Costa-Castelló, S. Malo, and R. Grinó, "High performance repetitive control of an active filter under varying network frequency," in *Proceedings of the 17th IFAC world congress*, 2008, pp. 3344–3349.
[28] T. Liu, D. Wang, and K. Zhou, "High-performance Grid Simulator using Parallel Structure Fractional Repetitive Control," *IEEE Trans. Power Electron.*, vol. PP, no. 99, pp. 1–1, 2015.
[29] B. Zhang, K. Zhou, and D. Wang, "Multirate Repetitive Control for PWM DC/AC Converters," *IEEE Trans. Ind. Electron.*, vol. 61, no. 6, pp. 2883–2890, Jun. 2014.
[30] C. James and N. Sadegh, "Synthesis and stability of a multirate repetitive learning controller," in *American Control Conference, 1999. Proceedings of the 1999*, 1999, vol. 1, pp. 358–362 vol.1.
[31] Z. Zou, K. Zhou, Z. Wang, and M. Cheng, "Fractional-order repetitive control of programmable AC power sources," *IET Power Electron.*, vol. 7, no. 2, pp. 431–438, Feb. 2014.
[32] T. I. Laakso, V. Valimaki, M. Karjalainen, and U. K. Laine, "Splitting the unit delay [FIR/all pass filters design]," *IEEE Signal Process. Mag.*, vol. 13, no. 1, pp. 30–60, Jan. 1996.
[33] S. Jiang, D. Cao, Y. Li, J. Liu, and F. Z. Peng, "Low-THD, Fast-Transient, and Cost-Effective Synchronous-Frame Repetitive Controller for Three-Phase UPS Inverters," *IEEE Trans. Power Electron.*, vol. 27, no. 6, pp. 2994–3005, Jun. 2012.
[34] L. Asiminoaei, F. Blaabjerg, and S. Hansen, "Detection is key-Harmonic detection methods for active power filter applications," *Ind. Appl. Mag. IEEE*, vol. 13, no. 4, pp. 22–33, 2007.
[35] C. J. Gajanayake, D. M. Vilathgamuwa, P. C. Loh, R. Teodorescu, and F. Blaabjerg, "Z-Source-Inverter-Based Flexible Distributed Generation System Solution for Grid Power Quality Improvement," *IEEE Trans. Energy Convers.*, vol. 24, no. 3, pp. 695–704, Sep. 2009.
[36] S.-K. Chung, "A phase tracking system for three phase utility interface inverters," *Power Electron. IEEE Trans. On*, vol. 15, no. 3, pp. 431–438, 2000.
[37] J. He and Y. W. Li, "Generalized closed-loop control schemes with embedded virtual impedances for voltage source converters with LC or LCL filters," *Power Electron. IEEE Trans. On*, vol. 27, no. 4, pp. 1850–1861, 2012.
[38] X. Wang, C. Bao, X. Ruan, W. Li, and D. Pan, "Design Considerations of Digitally-Controlled LCL-Filtered Inverter with Capacitor-Current-Feedback Active Damping," *IEEE J. Emerg. Sel. Top. Power Electron.*, vol. PP, no. 99, pp. 1–1, 2014.
[39] S. G. Parker, B. P. McGrath, and D. G. Holmes, "Regions of Active Damping Control for LCL Filters," *IEEE Trans. Ind. Appl.*, vol. 50, no. 1, pp. 424–432, Jan. 2014.
[40] V. Blasko and V. Kaura, "A novel control to actively damp resonance in input LC filter of a three-phase voltage source converter," *Ind. Appl. IEEE Trans. On*, vol. 33, no. 2, pp. 542–550, 1997.

Chuan Xie (S'11-M'16) received the B.S. degree in automation engineering from the University of Electronic Science and Technology of China, Chengdu, China, and the Ph.D. degree in power electronics from Zhejiang University, Hangzhou, China, in 2007 and 2012, respectively.

Since 2012, he was a lecturer with the School of Automation Engineering at University of Electronic Science and Technology of China. From May 2015 to May 2016, he was a Visiting Scholar at the Department of Energy Technology, Aalborg University.

His main research interests include digital control of power converters, grid synchronization technique, distributed generation systems, microgrids and power quality.

Xin Zhao (S'15) received the B.S. and M.S. degrees in Power Electronics & Electrical Drives from Northwestern Polytechnical University, Xi'an, China, in 2010 and 2013, respectively. He is currently pursuing the Ph.D. degree at the Department of Energy Technology, Aalborg University, Denmark.

His research interests include microgrids, distributed generation systems, control of power converters, and power quality issues in microgrids.

Mehdi Savaghebi (S'06-M'15-SM'15) was born in Karaj, Iran, in 1983. He received the B.Sc. degree from University of Tehran, Iran, in 2004 and the M.Sc. and Ph.D. degrees with highest honors from Iran University of Science and Technology, Tehran, Iran in 2006 and 2012, respectively, all in Electrical Engineering. From 2007 to 2014, he was a Lecturer in Electrical Engineering Department, Karaj Branch, Islamic Azad University where he taught various courses and conducted research on power systems and electrical machines. In 2010, he was a visiting Ph.D. Student with the Department of Energy Technology, Aalborg University, Aalborg, Denmark and with the Department of Automatic Control Systems and Computer Engineering, Technical University of Catalonia, Barcelona, Spain.

Currently, he is a Postdoctoral Fellow in the Department of Energy Technology, Aalborg University. His main research interests include distributed generation systems, microgrids, power quality and smart metering. Dr. Savaghebi is a member of Technical Committee of Renewable Energy Systems, IEEE Industrial Electronics Society and also IEEE Task Force on Microgrids Stability Analysis and Modeling.

Lexuan Meng (S'13-M'15) received the B.S. degree in Electrical Engineering and M.S. degree in Electrical Machine and Apparatus from Nanjing University of Aeronautics and Astronautics (NUAA), Nanjing, China, in 2009 and 2012, respectively, and the Ph.D. degree in power electronics from Aalborg University, Denmark, in 2015. He is currently working as postdoc in power electronic systems at Department of Energy Technology, Aalborg University, Denmark, as a member of the Denmark Microgrids Research Programme.

His research interests include the energy management system, secondary and tertiary control for microgrids concerning power quality regulation and optimization issues, as well as the applications of distributed control and communication algorithms.

Josep M. Guerrero (S'01-M'04-SM'08-F'15) received the B.S. degree in telecommunications engineering, the M.S. degree in electronics engineering, and the Ph.D. degree in power electronics from the Technical University of Catalonia, Barcelona, in 1997, 2000 and 2003, respectively. Since 2011, he has been a Full Professor with the Department of Energy Technology, Aalborg University, Denmark, where he is responsible for the Microgrid Research Program. From 2012 he is a guest Professor at the Chinese Academy of Science and the Nanjing University of Aeronautics and Astronautics; from 2014 he is chair Professor in Shandong University; and from 2015 he is a distinguished guest Professor in Hunan University.

His research interests is oriented to different microgrid aspects, including power electronics, distributed energy-storage systems, hierarchical and cooperative control, energy management systems, and optimization of microgrids and islanded minigrids. Prof. Guerrero is an Associate Editor for the IEEE TRANSACTIONS ON POWER ELECTRONICS, the IEEE TRANSACTIONS ON INDUSTRIAL ELECTRONICS, and the IEEE Industrial Electronics Magazine, and an Editor for the IEEE TRANSACTIONS on SMART GRID and IEEE TRANSACTIONS on ENERGY CONVERSION. He has been Guest Editor of the IEEE TRANSACTIONS ON POWER ELECTRONICS Special Issues: Power Electronics for Wind Energy Conversion and Power Electronics for Microgrids; the IEEE TRANSACTIONS ON INDUSTRIAL ELECTRONICS Special Sections: Uninterruptible Power Supplies systems, Renewable Energy Systems, Distributed Generation and Microgrids, and Industrial Applications and Implementation Issues of the Kalman Filter; and the IEEE TRANSACTIONS on SMART GRID Special Issue on Smart DC Distribution Systems. He was the chair of the Renewable Energy Systems Technical Committee of the IEEE Industrial Electronics Society. In 2014 and 2015 he was awarded by Thomson Reuters as Highly Cited Researcher, and in 2015 he was elevated as IEEE Fellow for his contributions on "distributed power systems and microgrids."

Juan C. Vasquez (M'12-SM'14) received the B.S. degree in electronics engineering from the Autonomous University of Manizales, Manizales, Colombia, and the Ph.D. degree in automatic control, robotics, and computer vision from the Technical University of Catalonia, Barcelona, Spain, in 2004 and 2009, respectively. He was with the Autonomous University of Manizales working as a teaching assistant and the Technical University of Catalonia as a Post-Doctoral Assistant in 2005 and 2008 respectively. In 2011, he was Assistant Professor and from 2014 he is working as an Associate Professor at the Department of Energy Technology, Aalborg University, Denmark where he is the Vice Programme Leader of the Microgrids Research Program. From Feb. 2015 to April. 2015 he was a Visiting Scholar at the Center of Power Electronics Systems (CPES) at Virginia Tech. His current research interests include operation, advanced hierarchical and cooperative control, optimization and energy management applied to distributed generation in AC and DC microgrids. He has authored and co-authored more than 100 technical papers only in Microgrids where 60 of them are published in international IEEE journals.

Dr. Vasquez is currently a member of the IEC System Evaluation Group SEG4 on LVDC Distribution and Safety for use in Developed and Developing Economies, the Renewable Energy Systems Technical Committee TC-RES in IEEE Industrial Electronics, PELS, IAS, and PES Societies.